Associations Between Retinal Pigment Epithelium and Drusen Volume Changes During the Lifecycle of Large Drusenoid Pigment Epithelial Detachments

Chandrakumar Balaratnasingam,[1–4] Lawrence A. Yannuzzi,[1,2] Christine A. Curcio,[5] William H. Morgan,[3] Giuseppe Querques,[6,7] Vittorio Capuano,[6] Eric Souied,[6,7] Jesse Jung,[1,2,8] and K. Bailey Freund[1–3]

[1]LuEsther T. Mertz Retinal Research Center, Manhattan Eye, Ear and Throat Hospital, New York, New York, United States
[2]Vitreous-Retina-Macula Consultants of New York, New York, United States
[3]Department of Ophthalmology, New York University School of Medicine, New York, New York, United States
[4]Department of Physiology and Pharmacology, Centre for Ophthalmology and Visual Science, Lions Eye Institute, University of Western Australia, Perth, Australia
[5]Department of Ophthalmology, University of Alabama School of Medicine, Birmingham, Alabama, United States
[6]Department of Ophthalmology, Hospital Intercommunal de Creteil, University Paris Est Creteil, Creteil, France
[7]Department of Ophthalmology, IRCCS San Raffaele Scientific Institute, University Vita-Salute San Raffaele, Milan, Italy
[8]East Bay Retina Consultants, Inc., Oakland, California, United States

Correspondence: K. Bailey Freund, Vitreous Retina Macula Consultants of New York, 460 Park Avenue, 5th Floor, New York, NY 10022, USA; kbfnyf@aol.com.

Submitted: April 25, 2016
Accepted: September 4, 2016

Citation: Balaratnasingam C, Yannuzzi LA, Curcio CA, et al. Associations between retinal pigment epithelium and drusen volume changes during the lifecycle of large drusenoid pigment epithelial detachments. *Invest Ophthalmol Vis Sci*. 2016;57:5479–5489. DOI:10.1167/iovs.16-19816

Purpose. Drusenoid pigment epithelial detachments (PEDs) are a defined path to atrophy in age-related macular degeneration (AMD). We analyzed the relationships between retinal pigment epithelium (RPE) and drusen volume changes during the PED lifecycle, using spectral-domain optical coherence tomography (SD-OCT).

Methods. Twenty-one cases of drusenoid PED tracked using SD-OCT through periods of growth and collapse were evaluated. Volumetric calculations and piece-wise linear regression analysis were used to determine the breakpoint between growth and collapse. Spectral-domain OCT scans were independently evaluated for the appearance of intraretinal hyperreflective foci, acquired vitelliform lesions (AVLs), and disruptions to the RPE+basal lamina band. Timing of these events with respect to the breakpoint was statistically evaluated. Morphometric characteristics of drusenoid PEDs were correlated with rate of PED collapse and final visual acuity.

Results. Mean age of subjects was 75.3 years and mean period of follow up was 4.1 years (median 4.5 years; range, 0.6–6.6 years). The lifecycle of drusenoid PEDs was asymmetric, in that the rate of collapse (0.199 mm^3/month) is significantly faster ($P < 0.001$) than the rate of growth (0.022 mm^3/month). Appearance of intraretinal hyperreflective foci and AVLs preceded the breakpoint (both $P < 0.001$). The timing of disruptions to the RPE+basal lamina band did not differ from the breakpoint ($P = 0.510$). Maximal height, volume, and diameter of drusenoid PEDs were inversely correlated with final visual acuity (all $P < 0.001$) and positively correlated with the rate of PED collapse (all $P < 0.001$).

Conclusions. Spectral-domain OCT signatures, plausibly attributable to anteriorly migrated RPE and disintegration of the RPE layer, precede or occur simultaneously with changes in volume of drusenoid PED during the lifecycle of this lesion.

Keywords: AMD, drusen, geographic atrophy, pigment epithelial detachment, retinal pigment epithelium

Macular drusen are a defining feature of AMD, a disease that accounts for severe visual loss in a considerable number of people over 65 years of age.[1] Drusenoid pigment epithelial detachments (PEDs) are characterized by displacement of the retinal pigment epithelium (RPE) away from Bruch's membrane (BrM) and are due to enlargement and/or coalescence of soft drusen.[2,3] The Age-Related Eye Disease Study defined a PED as a circumscribed, pale or white mound consisting of many large or confluent drusen that was at least 350 μm on the narrowest diameter and appeared elevated on stereoscopic color photographs.[2] Roquet et al.,[4] also using color photographs, set a size criterion of half-a-disk-diameter. In a recent multimodal imaging review, Mrejen et al.[3] defined drusenoid PEDs as structures where the detached RPE has a smooth or undulating contour on spectral-domain optical coherence tomography (SD-OCT) with moderate to high internal reflectivity. Drusenoid PEDs are well-demarcated precursors to atrophy in a subset of AMD patients.[4,5] However, the quantitative properties of the PED lifecycle and the cascade of RPE changes that underlie vision loss during this process remain unclear.[4,5]

Cells of the RPE layer are critically linked to retinal health and disease.[6,7] The RPE performs numerous functions essential

Investigative Ophthalmology & Visual Science

Table 1. Summary of Spectral-Domain Optical Coherence Tomography Imaging Protocol

Measured Parameters	Mean	Median	Minimum	Maximum
Raster pattern°	–	20 × 15 (5.6 × 4.2 mm)	15 × 15 (4.3 × 4.3 mm)	30 × 20 (8.9 × 5.9 mm)
Distance between individual B scans, μm	202.9 ± 58.9	235.5	116	255
Number of B scans per OCT volume	26.6 ± 8.9	25	19	49
A scan average (ART)	18.5 ± 10.9	15.5	9	60
Total number of imaging sessions per patient	20.3 ± 16.8	16	6	74
Interval between scans, mo	3.2 ± 1.7	2.9	1.1	6.6

to the photoreceptors and choroid, including phagocytosis of photoreceptor outer segments, absorption of excess light, processing of retinoids for phototransduction, maintenance of the outer blood–retina barrier, and secretion of growth factors, cytokines, and lipoprotein particles.[8–11] New information from comprehensive high-resolution histology is prompting a re-examination of RPE fate in the transition to atrophy in AMD.[12–15] These recent imaging–histology correlation studies have shown that a range of RPE activities are visible on optimized structural SD-OCT.

A limitation of histologic studies is that they provide structural information from only a single time-point in the disease course, yet such studies can facilitate use of SD-OCT information from clinic populations to study RPE changes as a function of time. The current report quantifies the timeline of drusenoid PED growth and collapse using high-resolution SD-OCT imaging. Retinal pigment epithelial changes that are associated with volumetric alterations during the PED lifecycle are also defined. Finally, this report identifies morphometric properties of drusenoid PEDs that are significant prognosticators of poor final visual acuity.

Methods

This study followed the Tenets of the Declaration of Helsinki and was approved by the Western institutional review board.

Patient Inclusion Criteria

Large drusenoid PEDs that were judged to be morphometrically similar to a forthcoming imaging–histology correlation of a donor eye (maximum diameter of base, 1916 μm, and maximum height of dome, 432 μm) were included in this study (illustrative case shown in Fig. 1). Another reason for evaluating large drusenoid PEDs in this study is because they are straightforward to track on OCT and demonstrate highly reproducible volumetric measurements (as described below). Only cases where SD-OCT imaging data was available from the baseline visit (first clinic visit) to the time of PED collapse were included for quantitative analysis in this study. Cases were selected in a retrospective manner from a consecutive series of PEDs seen between June 2015 and January 2016 by two retina specialists (LAY and KBF) at the Vitreous Retina Macula Consultants of New York. In those patients with bilateral drusenoid PEDs, a single eye was selected at random for inclusion into this study. Exclusion criteria included: (1) choroidal neovascularization confirmed with SD-OCT and dye angiography (fluorescein or indocyanine green), (2) retinal artery/vein occlusion, diabetic retinopathy, previous vitreoretinal surgery, and pathologic myopia, (3) geographic atrophy at baseline visit, (4) prior ocular therapies such as laser photocoagulation or intravitreal therapy, (5) PEDs due to other causes such as central serous chorioretinopathy and polypoidal choroidal vasculopathy, (6) inability to visualize BrM on SD-OCT, and (7) fewer than six OCT volume scans performed between baseline visit to the time of PED collapse.

Imaging

Color photography, fluorescein angiography (FA), and indocyanine green angiography (ICGA) images were acquired using the Topcon TRC-50XF fundus camera (Topcon Medical Systems, Paramus, NJ, USA). Fundus autofluorescence (FAF) images were obtained using the Spectralis HRA + OCT (Heidelberg Engineering, Heidelberg, Germany) or the Topcon TRC-50XF fundus camera (Topcon Medical Systems), respectively. All eyes underwent SD-OCT imaging using the Spectralis OCT (Heidelberg Engineering) at each visit. Eye tracking and image registration functions were enabled for all image acquisitions. The SD-OCT scan protocol for the cohort is summarized in Table 1.

SD-OCT Definitions for Outer Retinal Bands and Drusenoid Pigment Epithelial Detachment

In a healthy eye the fourth outer retinal hyperreflective band includes the RPE and BrM.[16,17] In a PED, by definition the RPE is separated from BrM and therefore it is incorrect to call the hyperreflective band that anteriorly delimits a PED the RPE-BrM. When the RPE is separated from BrM in the course of histologic preparation, either a basal lamina of 0.15-μm thickness or basal laminar deposit (BLamD) of variable thickness adheres to the cells and not to BrM, suggesting a natural cleavage plane between the RPE basal lamina and the inner collagenous layer of BrM.[18] In this study, we use the designation RPE+basal laminar (BL) to indicate the fourth outer retinal hyperreflective band in drusenoid PED.

Quantitative Volumetric Analysis of Drusenoid Pigment Epithelial Detachments

The PED volume at each visit was determined by applying the Cavalieri principle of stereological analysis to SD-OCT volumetric data (Fig. 2).[19] All measurements were attained using a 1:1 micron scaled image on SD-OCT software. Pigment epithelial detachment volume was determined using the following steps: (1) the area between the outer RPE+BL boundary and inner boundary of BrM for each slice in the PED volume scan was calculated using manual planimetry, (2) the volume between two adjacent OCT slices (herein called a segment) was then determined using this equation:

$$d\left(\frac{A_x + A_{x+1}}{2}\right) \quad (1)$$

where: d = distance between adjacent slices in μm, A = Area between the RPE+BL and BrM in μm^2, and x = OCT slice number.

(3) Total PED volume was calculated by summing the volumes of individual segments. The number of segments in the OCT volume was $(n - 1)$, where n = total number of slices that spanned the PED. Plots of PED volume versus time were then generated (Fig. 3). For eight eyes, volumetric measurements were repeated three times, on different days, and the

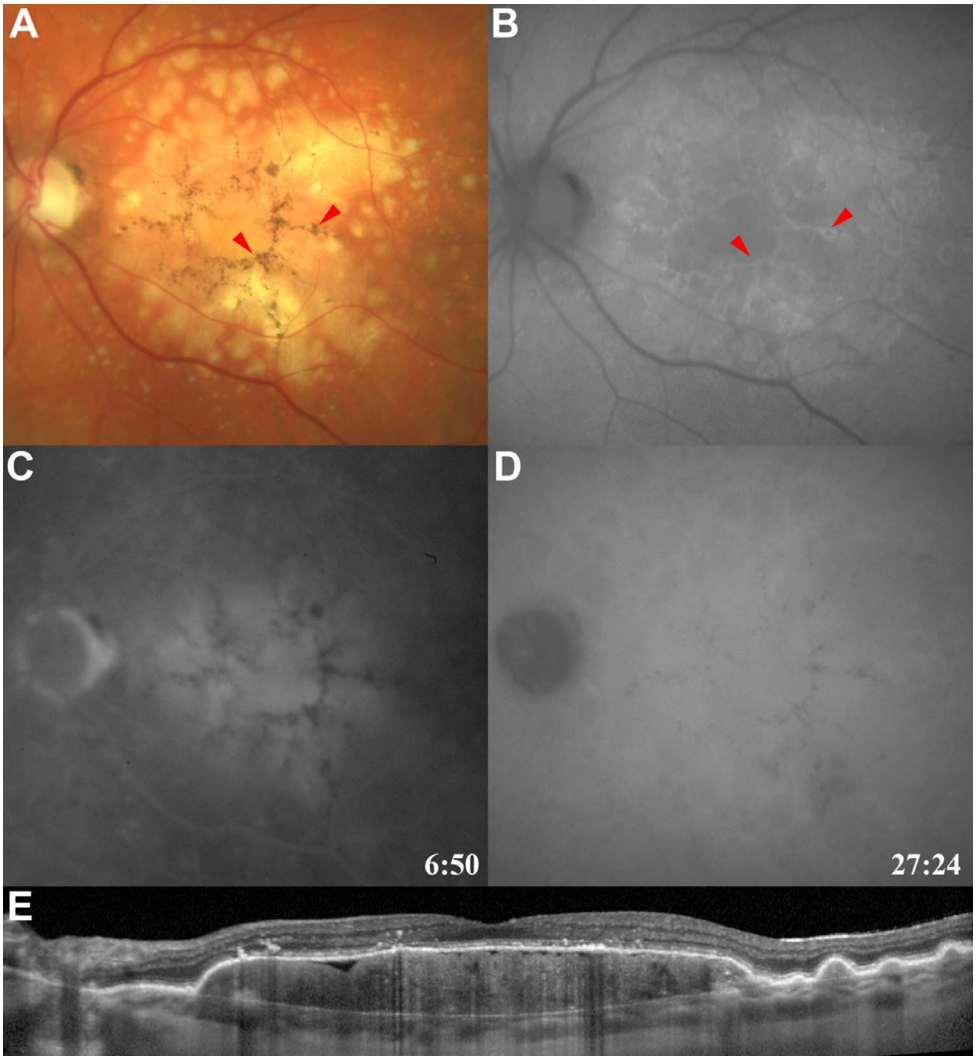

Figure 1. Clinical features of drusenoid PED. Drusenoid PEDs appeared as pale-yellow, subretinal pigment epithelial lesions with smooth or scalloped borders (**A**). Hyperpigmentation was commonly seen within the PED (*red arrowheads*) in regions that commonly correlated to areas of hyperautofluorescence on FAF imaging (**B**). Choroidal neovascularization was excluded using FA (**C**) and/or ICGA (**D**). Spectral-domain optical coherence tomography (**E**) demonstrates confluent elevation of the RPE and associated basal lamina with a relatively homogeneous hyperreflectivity pattern within the PED.

coefficient of variation was determined to measure the reproducibility of manual tracings. For these eyes, the mean of the three measurements was used for plots of PED volume versus time.

The following measurements were also attained at the visit where the volume of the PED was calculated to be greatest (Fig. 2):

1. Maximal diameter: defined as the greatest PED base diameter using BrM as the reference plane.
2. Maximal height: defined as the greatest distance between BrM and the outer boundary of the RPE+BL.
3. Maximal angle between RPE+BL and BrM: defined as the greatest angle within the entire volume scan, on both nasal and temporal aspects.

Pigment epithelial detachment area, height, and diameter measurements were determined using the contained software (Spectralis Viewing Module 4.0.0.0; Heidelberg Engineering), as was baseline central subfoveal choroidal thickness. Angle measurements were determined using Image J (version 1.43; http://imagej.nih.gov/ij/; provided in the public domain by the National Institutes of Health, Bethesda, MD, USA) following exportation of tif files.

Qualitative Evaluation of Pigment Epithelial Detachment and Outer Retinal Changes

Spectral-domain OCT volumetric scans were analyzed in a masked fashion for the following RPE structural changes:

1. Intraretinal hyperreflective foci: our recent histology-OCT correlation study demonstrated that intraretinal hyperreflective foci overlying drusenoid PEDs correspond to RPE cells, either singly or in groups.[14,15] The time point at which intraretinal hyperreflective foci on SD-OCT were first observed was recorded.
2. Disruptions to the RPE+BL band with associated increased light transmission (hypertransmission) through the PED into the choroid. Hypertransmission below the RPE is considered a reliable indicator of absence of the RPE layer, in geographic atrophy.[20–22] The time point at which disruptions to the RPE+BL band first occurred and their location in the PED dome (apex or

Investigative Ophthalmology & Visual Science

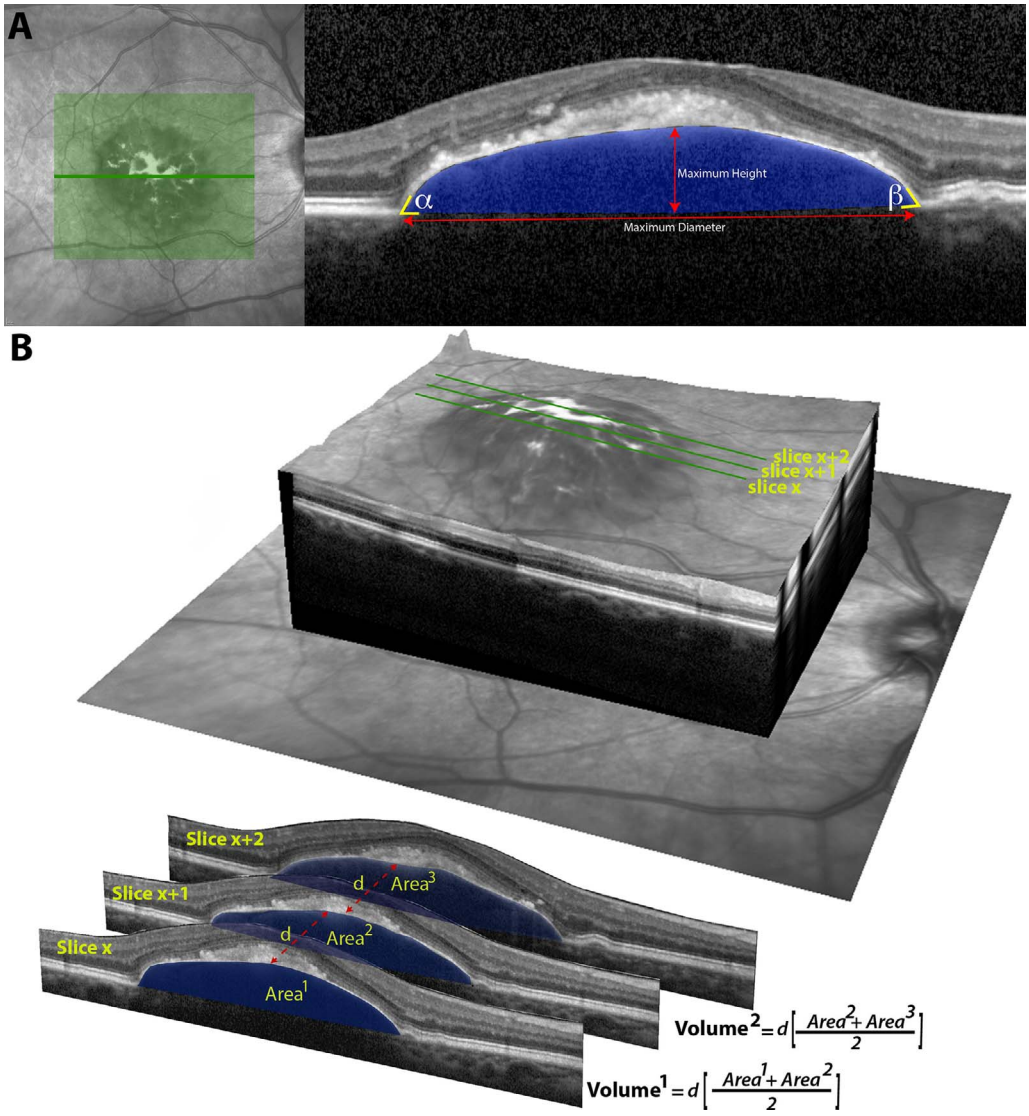

Figure 2. Quantifying morphometric and volumetric characteristics of drusenoid PEDs. A single SD-OCT B-scan (**A**) is used to illustrate the measurements that were acquired from the PED, which included maximum height and diameter. The angle of intersection between the RPE+BL band and BrM in the temporal (α) and nasal (β) margins of the PED was also determined. Manual tracing of Bruch's membrane and the outer margins of the RPE+BL band was used to calculate the cross-sectional area (*blue shade*) of the drusenoid PED. Area measurements from each slice in the OCT volume scan were then used to perform volumetric calculations (**B**). Three contiguous OCT slices illustrate the application of the Cavalieri principle in stereology for calculating volume. The volume of a segment, defined as the volume between two contiguous OCT slices, was determined by averaging the area of the drusenoid PED in the two slices and multiplying it by the distance (*d*) separating the slices. Summation of volumetric measurements from each segment allowed calculation of the entire volume of the PED.

base) was recorded. An RPE disruption at the base was defined as one that involved the point of intersection between attached and detached portions of the RPE+BL band. All other disruptions were defined as being at the apex. The size of these disruptions was measured with calipers available in the OCT software.

3. The occurrence of acquired vitelliform lesions: the multimodal imaging definition of AVL of Freund et al.[23] was used in this study. Specifically, the ophthalmoscopic and SD-OCT diagnoses of vitelliform material were based on the presence of yellowish deposits in the subretinal space and hyperreflective material above the RPE band, respectively. On FAF imaging, vitelliform material was defined by areas of hyperautofluorescence that correlated with the sites where vitelliform material was seen on color fundus and SD-OCT images. Acquired vitelliform lesions are comprised of sloughed RPE cells, RPE-derived organelles in the extracellular space, and outer segment debris.[15] The time point at which AVLs were first observed was recorded.

Statistical Analysis

Statistical analysis was performed using SPSS Version 21 (IBM Corp., Armonk, NY, USA) and R.[24] Piece-wise linear regression analysis using the SiZer package in R was used to identify significant slope change in the curves depicting PED volume as a function of time. The point of significant change in slope is herein referred to as the 'breakpoint' of the drusenoid PED lifecycle. The absolute value of the gradient of the slopes on either side of the breakpoint, representing the rate of PED volume increase and rate of PED collapse, respectively, were

Investigative Ophthalmology & Visual Science

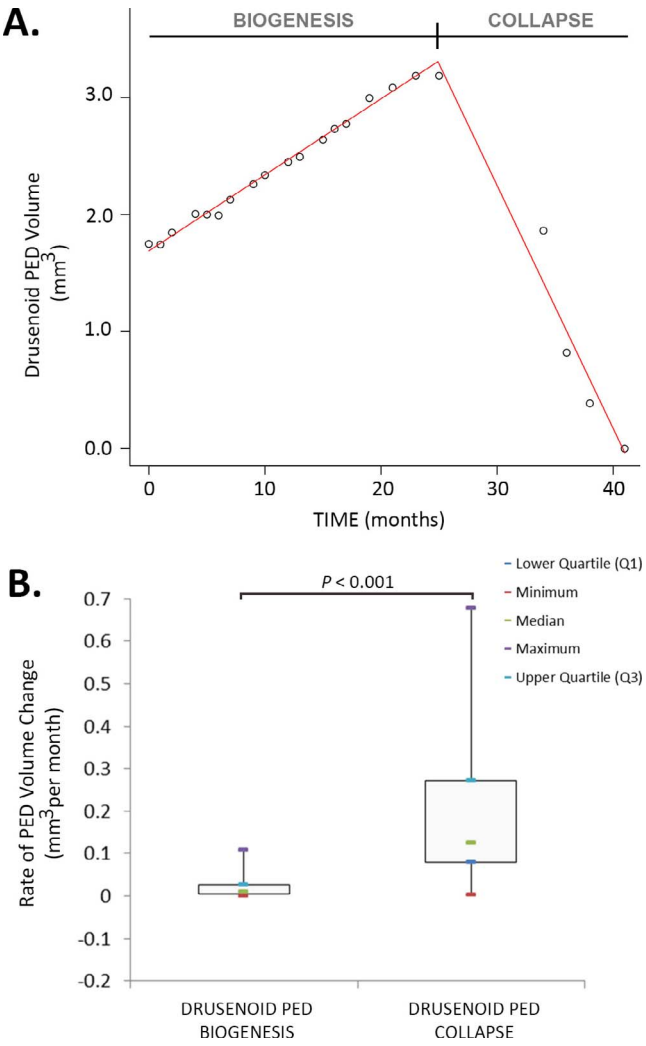

Figure 3. Drusenoid PED lifecycle. An illustrative plot of PED volume as a function of time is provided from a 72-year-old patient that was monitored over a period of 41 months (**A**). Lines of best fit, as determined by piece-wise linear regression analysis, are shown in *red*. Note the significant break point at 23 months where the gradient of the slope changes from positive to negative. Comparisons of the rate of drusenoid PED biogenesis (formation) and collapse in the cohort demonstrates a significant difference (**B**). The absolute value of the gradient of the slope for PED collapse is significantly greater than PED biogenesis. *Box* and *whisker plots* are used to summarize the rates of PED formation and collapse.

compared using a 2-sample *t*-test. *T*-tests were also used to compare the time of first occurrence of intraretinal hyperreflective foci, the time of first occurrence of RPE+BL band disruption, the time of first occurrence of AVLs, and the time of slope changes on the PED volume curve. Pearson's or Spearman's correlation was used to evaluate relationships between PED measurements including maximal height, maximal diameter, maximal volume, temporal angle, nasal angle, baseline visual acuity, and the rate of drusen volume decrease and logMAR final visual acuity. A P value less than 0.050 was considered significant. Quantitative results are expressed as mean ± SEM.

Results

General

A total of 216 eyes from 121 patients were reviewed of which 21 eyes from 21 patients met the inclusion criteria for this study. All eyes were graded as intermediate AMD at baseline visit. An illustrative case of a study eye is presented in Figure 1. On ophthalmoscopy, drusenoid PEDs appeared as yellow lesions with smooth or scalloped borders. Areas of RPE hyperpigmentation were seen on the PED surfaces, and these regions typically appeared hyperautofluorescent on FAF imaging. All patients were imaged with FA, and 10 patients were also imaged with ICGA. Fluorescein angiography demonstrated hyperfluorescence at the site of the PED that was more intense in the late stages of the angiogram, but did not extend beyond its margins. Areas of RPE hyperpigmentation appeared hypofluorescent on FA. On ICGA there was obscuration of the choroidal vessels at the site of the PED and hypofluorescence at sites of RPE hyperpigmentation.

Mean age of subjects was 75.3 ± 8.7 years (range, 56–91 years). The cohort comprised of 16 females, 5 males, 9 right eyes, and 12 left eyes. Mean time-period between the first OCT scan and last OCT scan was 4.1 ± 1.7 years (median 4.5 years, range, 0.6–6.6 years). Mean best-corrected visual acuity at baseline visit was 0.22 logMAR (Snellen equivalent 20/33; range, 0.1–0.5 logMAR). Best-corrected visual acuity at final visit was higher on the logMAR scale, 0.8 logMAR (Snellen equivalent 20/127; range, 0–2.3 logMAR; $P < 0.001$). Mean subfoveal choroidal thickness was 216.3 ± 87.9 µm (Table 2).

Drusenoid PED Volume Changes Over Time

An illustrative plot of PED volume against time is provided in Figure 3. Mean coefficient of variation for repeated PED volume measurements from eight eyes was 0.14 ± 0.04. All PEDs demonstrated dynamic changes characterized by a phase where PED volume gradually increased followed by a period of rapid reduction in volume to a floor value of zero or almost zero (Fig. 3A). At the final visit, the PED volume was measured as 0 mm^3 in 16 of 21 eyes (76%) and less than 10% of maximal PED volume in the remaining five eyes. Piece-wise linear regression analysis identified a breakpoint where the slope changed significantly between periods of growth and collapse in all cases (Fig. 3A). The absolute value of the slope during PED collapse (0.199 ± 0.176 mm^3/month) was significantly greater than the absolute value of the slope during PED growth

Table 2. Summary of Morphometric Dimensions of Drusenoid Pigment Epithelial Detachment and Subfoveal Choroidal Thickness

Measured Parameters	Mean	Median	Minimum	Maximum
Maximal diameter, µm	2426.5 ± 1096.2	2525	904	4691
Maximal height, µm	352.9 ± 156.3	338	164	659
Maximal volume, mm^3	1.6 ± 1.8	0.8	0.1	6.8
Nasal angle, °	42.1 ± 13.6	37.9	24.8	71
Temporal Angle, °	43.3 ± 12.4	43.3	23.4	65.2
Subfoveal choroidal thickness, µm	212.7 ± 88.7	219	52	376

(0.022 ± 0.028 mm^3/month; $P < 0.001$; Fig. 3B). The mean period of time from baseline visit to the breakpoint of the PED drusen lifecycle was 23.5 ± 19.9 months (range, 3–61 months). The mean period of time from breakpoint to complete collapse of the PED was 10.4 ± 4.2 months (range, 5–18 months). Visual acuity between baseline and the visit of maximal PED volume was not significantly different ($P = 0.105$). Visual acuity at the final visit was significantly worse than baseline visit and the visit where PED volume was maximal (both $P \leq 0.021$).

RPE Changes During the Lifecycle of Drusenoid PEDs

The relationships between changes to the RPE-BL band, as seen on SD-OCT, and volume changes during the drusenoid PED lifecycle are illustrated in Figure 4. Intraretinal hyperreflective foci were identified in all eyes (mean time of 4.1 ± 15.4 months from baseline visit), AVLs were seen in 66.7% of eyes (3.8 ± 13.4 months from baseline visit) and disruption of the RPE+BL band was seen in 81.0% of eyes (230.9 ± 106.3 months from baseline visit). The time point at which intraretinal hyperreflective foci were first observed did not differ from the time point when AVLs were first seen ($P = 0.950$). The time points at which intraretinal hyperreflective foci and AVLs were first observed was significantly earlier than the time point where disruption of the RPE+BL was first observed ($P = 0.004$ and $P = 0.005$, respectively).

Intraretinal hyperreflective foci were seen on average 19.4 ± 17.0 months before the breakpoint of the drusenoid PED lifecycle ($P = 0.001$). Acquired vitelliform lesions occurred on average 15.6 ± 15.9 months before the breakpoint of the drusenoid PED lifecycle ($P = 0.002$). Disruptions in the RPE+BL band were first observed a mean period of 3.7 ± 10.4 months before the breakpoint of the drusenoid PED lifecycle but this difference was not significant ($P = 0.510$).

Of the eyes with disruptions to the RPE+BL band, 76.5% of cases demonstrated disruptions at the apex of the PED only, while 23.5% demonstrated disruptions to the apex and base of the PED (Fig. 5). The mean length of RPE+BL disruptions was 230.9 ± 106.3 μm (range, 94–434 μm). There was no evidence of lateral or anterior retraction of the RPE adjacent to the area of RPE+BL defect. Disruptions were associated with hypertransmission below the RPE (Fig. 5).

Correlations Between PED Morphometry, Final Visual Acuity, and Rate of Collapse

Maximal PED morphometric measurements for each case are summarized in Table 2. Shapiro-Wilk normality testing demonstrated that data for maximal PED height and volume were not normally distributed (both $P \leq 0.013$) while maximal PED diameter was normally distributed ($P = 0.076$). Maximal PED diameter ($P < 0.001$; $r = -0.767$), maximal PED height ($P < 0.001$; $r = -0.724$), and maximal PED volume ($P < 0.001$; $r = -0.866$) were positively correlated with the rate of drusenoid PED collapse (Fig. 6). Baseline visual acuity ($P = 0.336$), nasal angle of PED ($P = 0.641$; $r = -0.111$), and temporal angle of PED ($P = 0.443$; $r = -0.182$) were not correlated with the rate of drusenoid PED collapse.

Maximal PED diameter ($P < 0.001$; $r = 0.685$), maximal PED height ($P < 0.001$; $r = 0.601$), and maximal PED volume ($P < 0.001$; $r = 0.723$) were inversely correlated with final visual acuity (Fig. 7). Baseline visual acuity ($P = 0.851$), nasal angle of PED ($P = 0.268$), and temporal angle of PED ($P = 0.294$) were not correlated with final visual acuity (Fig. 7).

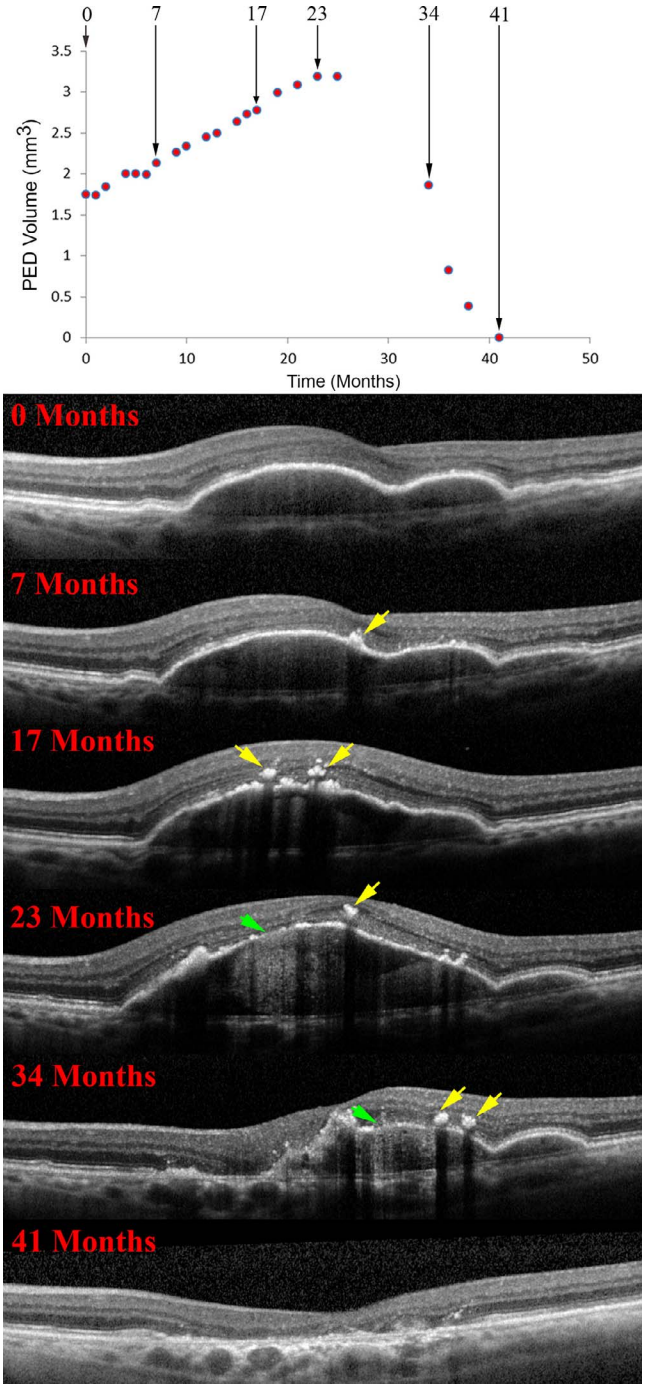

Figure 4. Retinal pigment epithelium changes and its relationship to the drusenoid PED lifecycle. Spectral-domain OCT images from the same patient as shown in Figure 3 illustrate RPE changes at different time-points. Intraretinal hyperreflective foci is first noted at 7 months and is seen as a localized hyperreflective lesion arising from the RPE+BL band (*yellow arrows*). At 23 months, disruptions to the RPE+BL band (*green arrow*) with increased light transmission (hypertransmission) to the choroid are evident, followed by a relatively rapid reduction in PED volume until 41 months. An acquired vitelliform lesion is not seen in this case but was noted to precede PED collapse in 66.7% of the study cases.

Investigative Ophthalmology & Visual Science

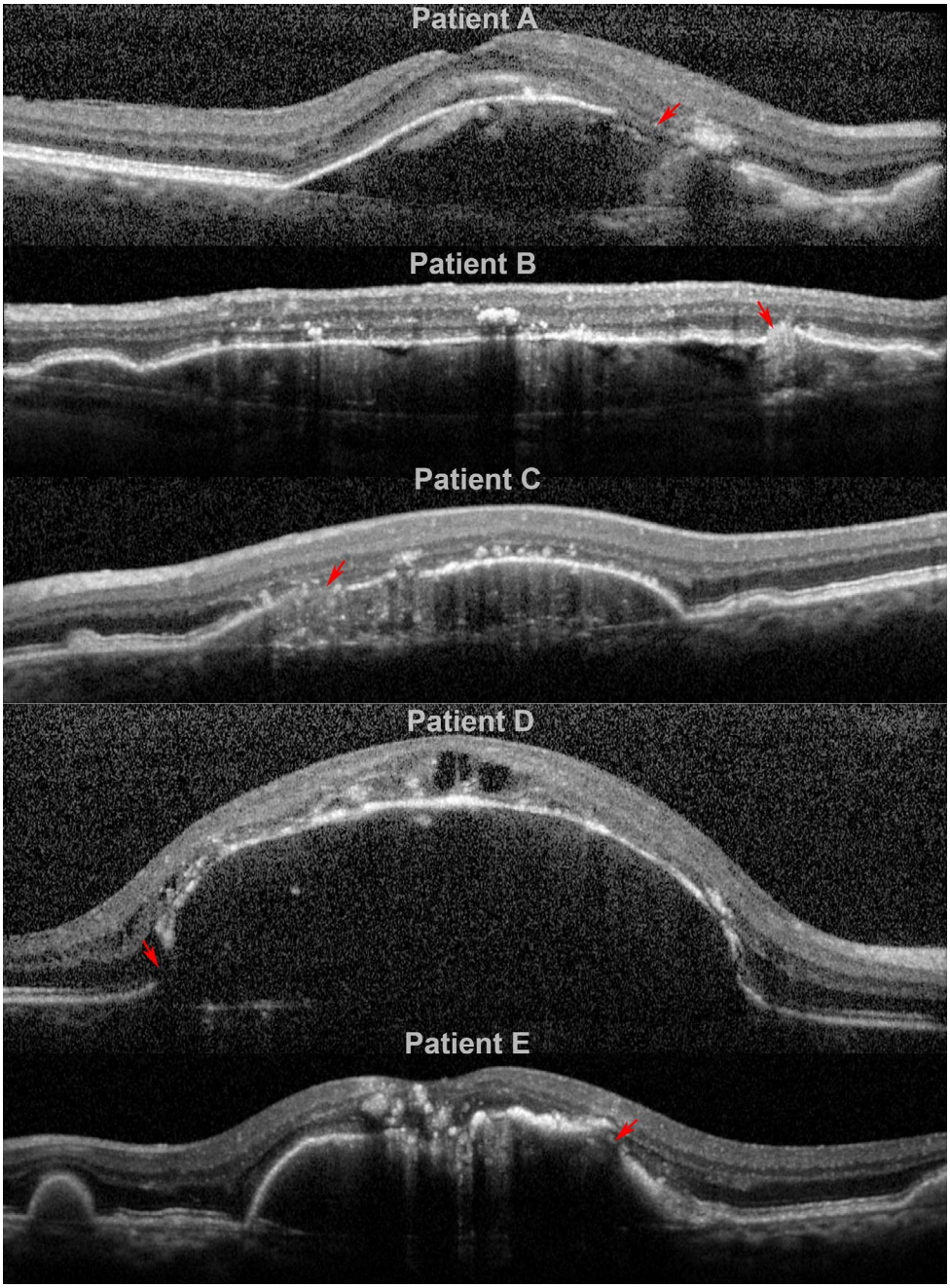

Figure 5. Spectrum of RPE+BL disruptions during the drusenoid PED lifecycle. Spectral-domain OCT images from different patients (**A**–**E**) demonstrate areas of RPE+BL disruption (*red arrows*) with hypertransmission to the choroid. Patients A, B, C and E demonstrate disruptions at the apex of the PED while Patient D demonstrates a disruption at the base of the PED.

Discussion

Drusenoid PEDs are a recognized phenotypic manifestation of nonneovascular AMD that are associated with increased risk of progression to geographic atrophy.[4,5] Understanding the temporal properties of the PED lifecycle is therefore important as it may identify biomarkers that can be used as clinical trial endpoints to guide treatment and prevent irreversible visual loss. This study quantified the lifecycle of large drusenoid PEDs based on longitudinal follow-up with structural SD-OCT. Piecewise linear regression analysis revealed that the growth and collapse phases of the drusenoid PED lifecycle are asymmetrical; the rate of drusenoid PED collapse (mean 0.2 mm^3/month) was significantly faster than the rate of PED growth (mean 0.02 mm^3/month). Important determinants of the rate of drusenoid PED collapse included maximal PED volume, height, and diameter. Larger drusenoid PEDs demonstrated a faster rate of collapse. Recently, Schlanitz and colleagues[25] evaluated drusen volume changes using SD-OCT and polarization-sensitive OCT in eyes with drusen of AREDS categories 2 and 3. These authors showed that the drusen lifecycle was also comprised of periods of growth and regression. The relationships between RPE and drusen volume changes were not explored in that study, however. Collectively, the findings of their study and this report demonstrate a degree of overlap in the natural history of drusen and drusenoid PEDs.

Investigative Ophthalmology & Visual Science

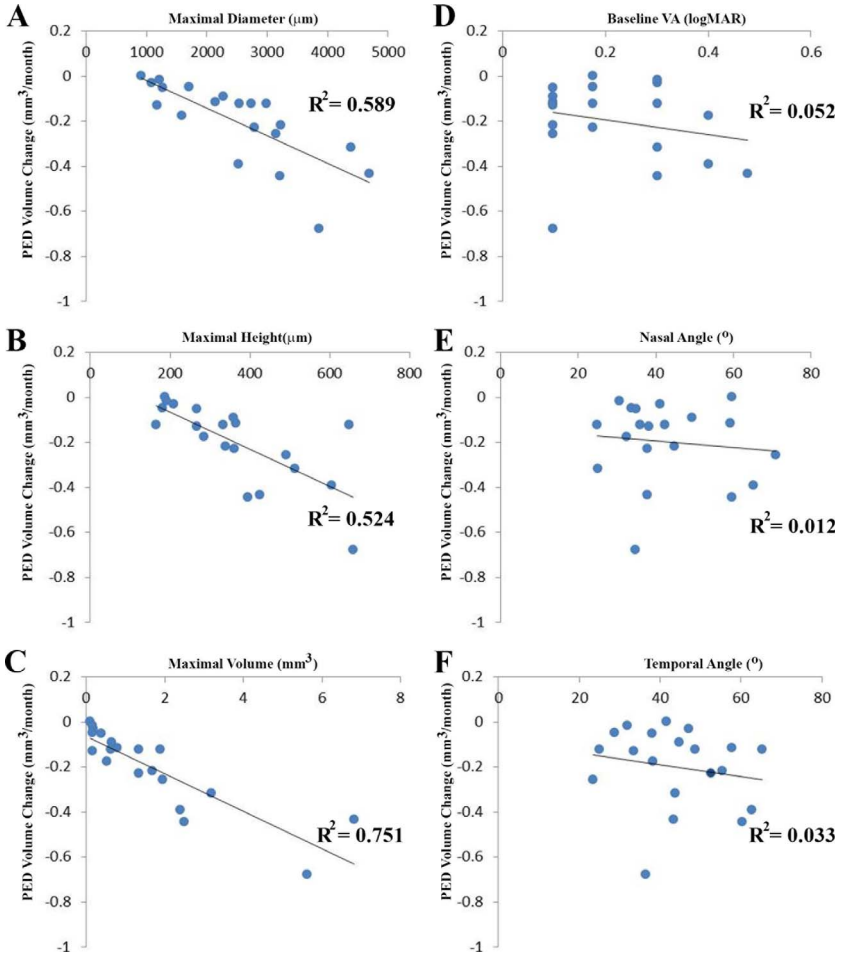

Figure 6. Predictors of final visual acuity (VA) following drusenoid PED collapse. Scatter plots demonstrate that PED diameter (**A**), PED height (**B**), and PED volume (**C**) are significantly correlated with final visual acuity (all $P < 0.001$). Baseline VA (**D**), nasal angle of PED (**E**), and temporal angle of PED (**F**) were not correlated to final VA. The best-fit trend line and R^2 are presented on each plot.

Structural and functional changes to RPE cells are inherently linked to the pathophysiological cascades underlying atrophy and photoreceptor loss due to AMD. Intraretinal hyperreflective foci are frequently seen on SD-OCT in eyes with AMD, yet there has been some controversy regarding their cellular origin. In 2006, Peirroni et al.[26] proposed that hyperreflective foci overlying drusenoid PEDs signified RPE migration into the retina. Framme and colleagues[27,28] proposed that these features in AMD eyes reflect leucocytes or migrating RPE cells. High-resolution studies of eyes with AMD recently completed by Curcio and colleagues,[29] including two cases with large subfoveal serous and hemorrhagic PED, established a histologic basis for RPE morphology visible in SD-OCT.[7,14,15,29] These histopathology-OCT correlations demonstrated that (1) hyperreflective intraretinal foci represent fully pigmented and nucleated RPE cells apparently migrating in an anterior direction, and (2) focal thickening of the RPE+BL band resembling AVLs represent subretinal, extracellular plaques of numerous RPE granules, and some outer segment debris.

The present study delineated the time course of RPE changes during the drusenoid PED lifecycle using these previously determined OCT-histologic correlations. All eyes in our cohort demonstrated one or more RPE structural alterations prior to PED collapse including appearance of intraretinal hyperreflective foci, formation of AVLs, and/or disruption of the RPE+BL band. Retinal pigment epithelial changes that were identified in this study may represent distinct manifestations of different RPE degenerative pathways (as hypothesized[30]) or different manifestations of a time-dependent continuum. Mrejen et al.[3] proposed that RPE atrophy in drusenoid PEDs was due to prolonged displacement from the choriocapillaris, its major source of nutrition. This may be one reason why disruptions to the RPE+BL band were frequently seen at the apex of the PED, the point of greatest separation from the choriocapillaris. It is important to distinguish disruptions to the RPE+BL band in drusenoid PEDs from RPE rips, which are a recognized complication of neovascular AMD.[31–33] Retinal pigment epithelial tears in neovascular AMD are due to abnormal tractional forces acting on the PED and typically occur at the margin, which is the point of greatest mechanical stress in a dome-shaped structure.[32,33] Unlike RPE tears due to neovascular AMD, rippling or retraction of the RPE was not seen at sites of RPE+BL disruption in this study.[33,34] Our findings therefore suggest that RPE disruptions in drusenoid PEDs are principally due to activities intrinsic to RPE cells such as necroptosis, apoptosis, and migration, in response to environmental signals, rather than mechanical forces. Ouyang and colleagues[35] performed longitudinal evaluations of drusenoid lesions and demonstrated that intraretinal hyperreflective lesions increased the risk of progression to atrophy. The findings of our study support this conclusion. However, we emphasize that anterior migration of RPE cells was not predictive of poor visual acuity in all eyes as some of the cases in our cohort retained a vision of 20/20

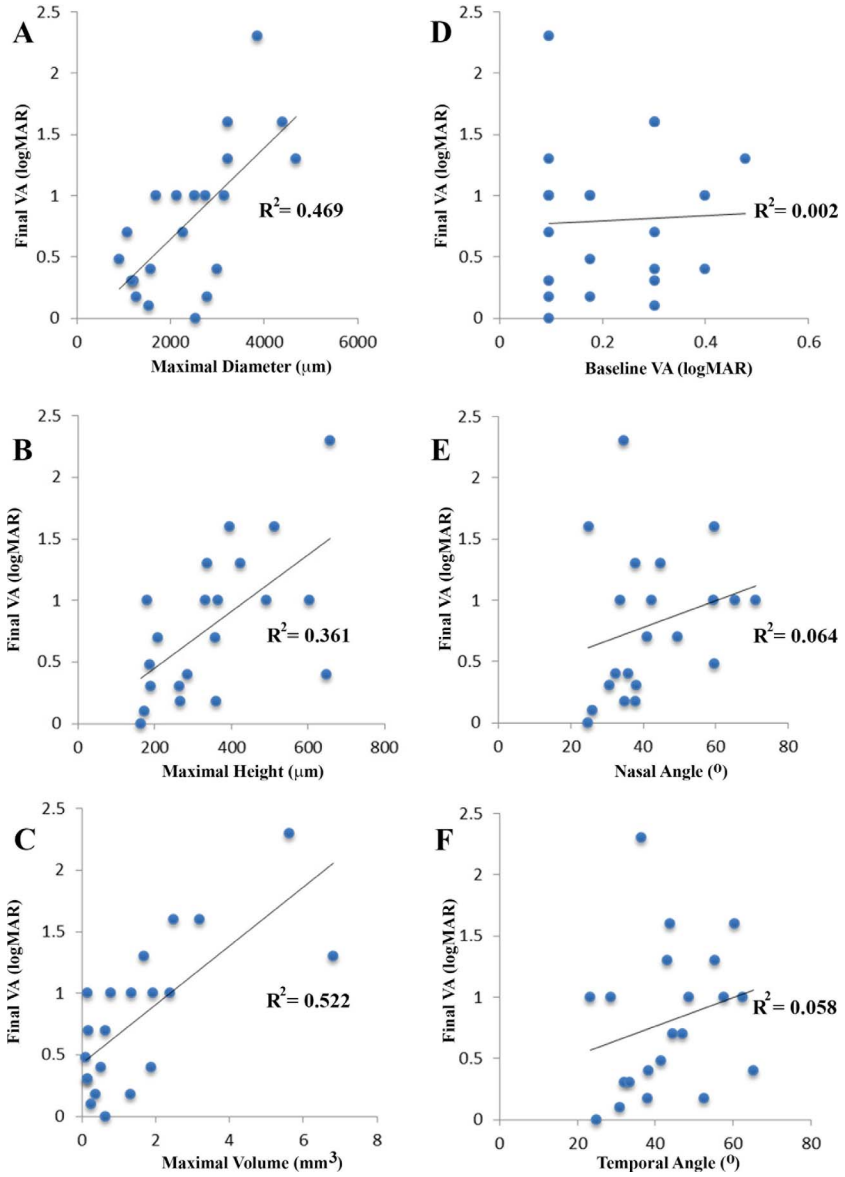

Figure 7. Correlations between drusenoid PED morphometry and final VA. Maximal PED diameter (**A**), height (**B**), and volume (**C**) are significantly correlated with final VA. Correlations between baseline VA (**D**), nasal angle (**E**), temporal angle (**F**), and final VA were not identified. The best-fit trend line and R^2 are presented on each plot.

following collapse of the PED. Pathogenic mechanisms beyond anterior migration of RPE cells are therefore contributory to the development of geographic atrophy in AMD.

As RPE-derived molecules and multimolecular complexes are major druse components, it is plausible that dysfunction or loss of RPE cells is associated with a decline in drusen volume. Multiple lines of evidence suggest that soft drusen and basal linear deposit form because large cholesterol-rich lipoproteins containing apolipoproteins B and E are secreted from the basal surface of the RPE and accumulate throughout adulthood on the inner collagenous layer of aging BrM.[36,37] In our study, the breakpoint in the drusenoid PED life cycle coincided with the time where RPE+BL disruptions were observed. Thus, the presence of drusen may be a positive sign that RPE is healthy enough to continue secreting material and thus maintain the lesions. Sarks et al.[5] observed that RPE attenuation, as seen on FA and histology, was associated with the early stages of drusen regression. However, their report did not delineate temporal relationships between the RPE and drusenoid PED volume changes. Microglia and activated Müller cells have all been identified in lesion debris of atrophic AMD eyes[38–42] and in eyes treated by nanosecond laser for drusen abatement.[43] These cells may also share responsibility for clearing. Future research is needed to determine if PED collapse and loss of drusenoid material is due to reduced secretion by RPE, active removal of drusen constituents by scavenging cells, or both.

The inclusion criteria for this study ensured that we evaluated a population of PEDs rather than just large drusen. A considerable advantage with evaluating large drusenoid PEDs is fewer errors associated with image segmentation, particularly with respect to defining the boundary between the RPE+BL band and drusen.[44] Previous studies have shown that the boundaries of the RPE+BrM layer can be obscured on OCT due to noise and poor image quality, thus resulting in inaccuracies in drusen volume calculations.[45] The coefficient of variation for repeat measurements in this study was low (0.14 ± 0.04), suggesting that the methodology for volumetric analysis was reproducible. The inclusion criteria used in this

study, however, limits the degree to which these findings can be extrapolated to other pathways leading to atrophy, such as soft drusen in the absence of PED. Other limitations of this study include its limited sample size and the nonstandardized OCT imaging protocol. Nevertheless, our study represents the first attempt to link cellular-level changes in the RPE layer to the dynamism of drusenoid PED.

Acknowledgments

Supported by grants from the LuEsther T. Mertz Retinal Research Center, Manhattan Eye, Ear and Throat Hospital (New York, NY, USA), The Macula Foundation, Inc., (New York, NY, USA), the National Eye Institute (EY06109; Bethesda, MD, USA) Research to Prevent Blindness, Inc. (New York, NY, USA), EyeSight Foundation of Alabama (Birmingham, AL, USA), and The RANZCO Eye Foundation (New South Wales, Australia).

Disclosure: **C. Balaratnasingam**, None; **L.A. Yannuzzi**, Genentech (R); **C.A. Curcio**, Genentech (C, R), Novartis (C, R), Merck (C, R), Janssen Cell Therapy (C, R), Regeneron (C, R), Ora (C, R); **W.H. Morgan**, None; **G. Querques**, Alimera Sciences, Inc. (C, S), Allergan, Inc. (C, S), Bayer Schering Pharma (C, S), Novartis Pharmaceuticals Corporation, (C, S), Bausch&Lomb (C), Ophthotech (C); **V. Capuano**, None; **E. Souied**, Allergan (C, R, S), Bayer (C, R, S), Novartis (C, R, S), Bausch&Lomb (S); **J. Jung**, None; **K.B. Freund**, Genentech (C, R), Bayer HealthCare (C, R), Optovue (C, R), ThromboGenics (C, R), Ohr Pharmaceutical (C, R), Heidelberg Engineering (C, R)

References

1. Klein R, Klein BE, Tomany SC, Meuer SM, Huang GH. Ten-year incidence and progression of age-related maculopathy: the Beaver Dam Eye Study. *Ophthalmology*. 2002;109:1767–1779.
2. Cukras C, Agron E, Klein ML, et al. Natural history of drusenoid pigment epithelial detachment in age-related macular degeneration: Age-Related Eye Disease Study Report No. 28. *Ophthalmology*. 2010;117:489–499.
3. Mrejen S, Sarraf D, Mukkamala SK, Freund KB. Multimodal imaging of pigment epithelial detachment: a guide to evaluation. *Retina*. 2013;33:1735–1762.
4. Roquet W, Roudot-Thoraval F, Coscas G, Soubrane G. Clinical features of drusenoid pigment epithelial detachment in age related macular degeneration. *Br J Ophthalmol*. 2004;88:638–642.
5. Sarks JP, Sarks SH, Killingsworth MC. Evolution of geographic atrophy of the retinal pigment epithelium. *Eye*. 1988;2(pt 5):552–577.
6. Sparrow JR, Hicks D, Hamel CP. The retinal pigment epithelium in health and disease. *Curr Mol Med*. 2010;10:802–823.
7. Ach T, Tolstik E, Messinger JD, Zarubina AV, Heintzmann R, Curcio CA. Lipofuscin redistribution and loss accompanied by cytoskeletal stress in retinal pigment epithelium of eyes with age-related macular degeneration. *Invest Ophthalmol Vis Sci*. 2015;56:3242–3252.
8. Curcio CA, Johnson M, Huang JD, Aging Rudolf M. age-related macular degeneration, and the response-to-retention of apolipoprotein B-containing lipoproteins. *Prog Retin Eye Res*. 2009;28:393–422.
9. Rizzolo LJ, Peng S, Luo Y, Xiao W. Integration of tight junctions and claudins with the barrier functions of the retinal pigment epithelium. *Prog Retin Eye Res*. 2011;30:296–323.
10. Strauss O. The retinal pigment epithelium in visual function. *Physiol Rev*. 2005;85:845–881.
11. Shi G, Maminishkis A, Banzon T, et al. Control of chemokine gradients by the retinal pigment epithelium. *Invest Ophthalmol Vis Sci*. 2008;49:4620–4630.
12. Vogt SD, Curcio CA, Wang L, et al. Retinal pigment epithelial expression of complement regulator CD46 is altered early in the course of geographic atrophy. *Exp Eye Res*. 2011;93:413–423.
13. Zanzottera EC, Messinger JD, Ach T, Smith RT, Curcio CA. Subducted and Melanotic cells in advanced age-related macular degeneration are derived from retinal pigment epithelium. *Invest Ophthalmol Vis Sci*. 2015;56:3269–3278.
14. Zanzottera EC, Messinger JD, Ach T, Smith RT, Freund KB, Curcio CA. The project MACULA retinal pigment epithelium grading system for histology and optical coherence tomography in age-related macular degeneration. *Invest Ophthalmol Vis Sci*. 2015;56:3253–3268.
15. Chen KC, Jung JJ, Curcio CA, et al. Intraretinal hyperreflective foci in acquired vitelliform lesions of the macula: clinical and histologic study. *Am J Ophthalmol*. 2016;164:89–98.
16. Spaide RF, Curcio CA. Anatomical correlates to the bands seen in the outer retina by optical coherence tomography: literature review and model. *Retina*. 2011;31:1609–1619.
17. Staurenghi G, Sadda S, Chakravarthy U, Spaide RF; for the International Nomenclature for Optical Coherence Tomography Panel. Proposed lexicon for anatomic landmarks in normal posterior segment spectral-domain optical coherence tomography: the IN*OCT consensus. *Ophthalmology*. 2014;121:1572–1578.
18. Curcio CA, Balaratnasingam C, Messinger JD, Yannuzzi LA, Freund KB. Correlation of type 1 neovascularization associated with acquired vitelliform lesion in the setting of age-related macular degeneration. *Am J Ophthalmol*. 2015;160:1024–1033, e1023.
19. Prakash YS, Smithson KG, Sieck GC. Application of the Cavalieri principle in volume estimation using laser confocal microscopy. *Neuroimage*. 1994;1:325–333.
20. Sayegh RG, Simader C, Scheschy U, et al. A systematic comparison of spectral-domain optical coherence tomography and fundus autofluorescence in patients with geographic atrophy. *Ophthalmology*. 2011;118:1844–1851.
21. Wolf-Schnurrbusch UE, Enzmann V, Brinkmann CK, Wolf S. Morphologic changes in patients with geographic atrophy assessed with a novel spectral OCT-SLO combination. *Invest Ophthalmol Vis Sci*. 2008;49:3095–3099.
22. Yehoshua Z, de Amorim Garcia Filho CA, Nunes RP, et al. Comparison of geographic atrophy growth rates using different imaging modalities in the COMPLETE Study. *Ophthalmic Surg Lasers Imaging Retina*. 2015;46:413–422.
23. Freund KB, Laud K, Lima LH, Spaide RF, Zweifel S, Yannuzzi LA. Acquired vitelliform lesions: correlation of clinical findings and multiple imaging analyses. *Retina*. 2011;31:13–25.
24. R Core Team. R: A Language and Environment for Statistical Computing. Vienna: R Foundation for Statistical Computing; 2013.
25. Schlanitz FG, Baumann B, Kundi M, et al. Drusen volume development over time and its relevance to the course of age-related macular degeneration [published online ahead of print April 4 2016]. *Br J Ophthalmol*. doi: 10.1136/bjophthalmol-2016-308422.
26. Pieroni CG, Witkin AJ, Ko TH, et al. Ultrahigh resolution optical coherence tomography in non-exudative age related macular degeneration. *Br J Ophthalmol*. 2006;90:191–197.
27. Framme C, Wolf S, Wolf-Schnurrbusch U. Small dense particles in the retina observable by spectral-domain optical coherence tomography in age-related macular degeneration. *Invest Ophthalmol Vis Sci*. 2010;51:5965–5969.
28. Framme C, Schweizer P, Imesch M, Wolf S, Wolf-Schnurrbusch U. Behavior of SD-OCT-detected hyperreflective foci in the retina of anti-VEGF-treated patients with diabetic macular edema. *Invest Ophthalmol Vis Sci*. 2012;53:5814–5818.

29. Pang CE, Messinger JD, Zanzottera EC, Freund KB, Curcio CA. The onion sign in neovascular age-related macular degeneration represents cholesterol crystals. *Ophthalmology*. 2015; 122:2316–2326.
30. Zanzottera EC, Ach T, Huisingh C, Messinger JD, Spaide RF, Curcio CA. Visualizing retinal pigment epithelium phenotypes in the transition to geographic atrophy in age-related macular degeneration. *Retina*. In press.
31. Caramoy A, Kirchhof B, Fauser S. Retinal pigment epithelium tears secondary to age-related macular degeneration: a simultaneous confocal scanning laser ophthalmoscopy and spectral-domain optical coherence tomography study. *Arch Ophthalmol*. 2011;129:575–579.
32. Krishan NR, Chandra SR, Stevens TS. Diagnosis and pathogenesis of retinal pigment epithelial tears. *Am J Ophthalmol*. 1985;100:698–707.
33. Cantrill HL, Ramsay RC, Knobloch WH. Rips in the pigment epithelium. *Arch Ophthalmol*. 1983;101:1074–1079.
34. Sarraf D, Reddy S, Chiang A, Yu F, Jain A. A new grading system for retinal pigment epithelial tears. *Retina*. 2010;30:1039–1045.
35. Ouyang Y, Heussen FM, Hariri A, Keane PA, Sadda SR. Optical coherence tomography-based observation of the natural history of drusenoid lesion in eyes with dry age-related macular degeneration. *Ophthalmology*. 2013;120:2656–2665.
36. Pikuleva IA, Curcio CA. Cholesterol in the retina: the best is yet to come. *Prog Retin Eye Res*. 2014;41:64–89.
37. Curcio CA, Johnson M, Rudolf M, Huang JD. The oil spill in ageing Bruch membrane. *Br J Ophthalmol*. 2011;95:1638–1645.
38. Gupta N, Brown KE, Milam AH. Activated microglia in human retinitis pigmentosa, late-onset retinal degeneration, and age-related macular degeneration. *Exp Eye Res*. 2003;76:463–471.
39. Ma W, Coon S, Zhao L, Fariss RN, Wong WT. A2E accumulation influences retinal microglial activation and complement regulation. *Neurobiol Aging*. 2013;34:943–960.
40. Lad EM, Cousins SW, Van Arnam JS, Proia AD. Abundance of infiltrating CD163+ cells in the retina of postmortem eyes with dry and neovascular age-related macular degeneration. *Graefes Arch Clin Exp Ophthalmol*. 2015;253:1941–1945.
41. Guidry C, Medeiros NE, Curcio CA. Phenotypic variation of retinal pigment epithelium in age-related macular degeneration. *Invest Ophthalmol Vis Sci*. 2002;43:267–273.
42. Wu KH, Madigan MC, Billson FA, Penfold PL. Differential expression of GFAP in early v late AMD: a quantitative analysis. *Br J Ophthalmol*. 2003;87:1159–1166.
43. Jobling AI, Guymer RH, Vessey KA, et al. Nanosecond laser therapy reverses pathologic and molecular changes in age-related macular degeneration without retinal damage. *FASEB J*. 2015;29:696–710.
44. Penha FM, Rosenfeld PJ, Gregori G, et al. Quantitative imaging of retinal pigment epithelial detachments using spectral-domain optical coherence tomography. *Am J Ophthalmol*. 2012;153:515–523.
45. Chen Q, Leng T, Zheng L, et al. Automated drusen segmentation and quantification in SD-OCT images. *Med Image Anal*. 2013;17:1058–1072.

Investigative Ophthalmology & Visual Science